ARTICLE

A New Route to the Production and Nanoscale Patterning of Highly Smooth, Ultrathin Zirconium Oxide Films

Scott M. D. Watson, Karl S. Coleman,* and Amit K. Chakraborty

Department of Chemistry, Durham University, South Road, DH1 3LE, U.K.

ABSTRACT Metal-stabilized bilayers, prepared by the self-assembly of octadecyltrichorosilane on an oxidized silicon surface followed by the Langmuir—Blodgett deposition of a monolayer of octadecylphosphonic acid, have been used to generate 1.6 nanometer thick, highly uniform, zirconium oxide films following annealing. Patterning of the thin films on the nanometre scale was achieved using nanodisplacement methodology, by careful control of an atomic force microscope (AFM) probe, which allowed the selective removal of the upper leaflet of the bilayer.

KEYWORDS: zirconium oxide · AFM · nanoscale patterning · ultrathin films · Langmuir—Blodget · nanodisplacement · nanoshaving

Thin films of ZrO_2 have attracted much attention and can be used as coatings to prevent corrosion and promote thermal stability.[1] But perhaps the most promising application of ZrO_2 films is in the electronics industry as a replacement dielectric for SiO_2 or oxynitrides in complementary metal oxide semiconductor (CMOS) technology. The constant scaling down of transistors has necessarily led to a demand for reduced thickness gate dielectrics. The reduction of the standard gate dielectric SiO_2 to a thickness approaching 1.5 nm results in problems such as current leakage and electron channel mobility degradation which have an adverse effect on device performance.[2] Substantial effort has therefore focused on replacing the gate SiO_2 with other higher dielectric materials such as metal oxides. This raises other issues such as compatibility with silicon and the ability of the material to withstand the conditions of semiconductor processing. One metal oxide which may meet such requirements is zirconium oxide (ZrO_2), which has a high dielectric constant and is considered to be stable against silicidation and silicate formation to temperatures up to 900 °C.[3]

Several different methods for the production of thin ZrO_2 films have been reported in recent years, including chemical vapor deposition (CVD),[4] atomic layer chemical vapor deposition (ALCVD),[5] sol—gel synthesis,[6] electron beam deposition,[7] filtered cathodic vacuum arc (FCVA) deposition,[8] and sputtering.[9] Typically these processes have been used in the production of ZrO_2 films ranging from several to hundreds of nanometer thick, with a typical root-mean-square (rms) roughness of <1 nm.

Here we demonstrate a new approach for the production of highly smooth, nanometer-thick ZrO_2 films, by deposition of zirconium-stabilized "Langmuir—Blodgett" (LB) films of octadecylphosphonic acid (ODP-H_2) upon SiO_2 supports, Scheme 1. The use of multilayer LB films as precursors to metal oxide films has previously been employed in the production of Fe,[10] Cd,[11,12] Zn,[13] Ti,[14] and Y[15] oxide films, ranging from several to ten's of nanometers thick. Typically the metal ions are incorporated into the water subphase, prior to LB deposition, to allow binding of the ions to the "headgroups" of the constituent monolayer molecules. The metal oxide films are subsequently generated through plasma, UV, or high temperature treatment of the LB film. Similarly, preparation of Y_2O_3-stabilized ZrO_2 films (approximately 40 nm thick) by LB deposition have previously been reported, in which β-diketonate Zr and Y complexes are incorporated within the monolayer precursor solution, rather than in the water subphase.[16] To our knowledge there are no reported examples of the production, and subsequent nanoscale patterning, of ultrathin ZrO_2 films using LB film precursors.

RESULTS AND DISCUSSION

Langmuir—Blodgett Film Formation. Langmuir—Blodgett (LB) films of octadecylphosphonic acid stabilized with di-, tri-, and tetravalent metal ions have

*Address correspondence to k.s.coleman@durham.ac.uk.

Received for review August 2, 2007 and accepted March 20, 2008.

Published online April 4, 2008.
10.1021/nn700138q CCC: $40.75

© 2008 American Chemical Society

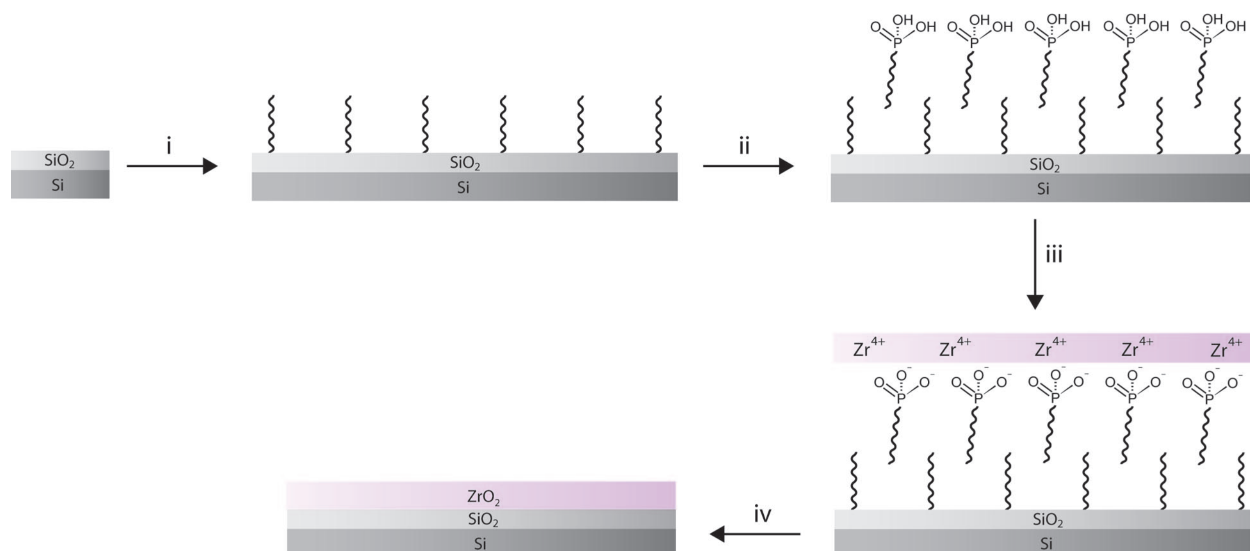

Scheme 1. Fabrication of ZrO_2 ultra-thin films: (i) self-assembly of octadecyltrichlorosilane; (ii) LB deposition of octadecylphosphonic acid; (iii) zirconium ion self-assembly; (iv) 500 °C.

received much attention, with the metal ions sandwiched between layers of organophosphate used as models or mimics for layered metal phosphonate lattice structures.[17] The preparation of ordered multilayer zirconium organophosphonate films by self-assembly[18–20] and a combination of LB deposition and inorganic self-assembly[21] have been reported. Using the method described by Talham *et al.*[21] we have deposited a single LB monolayer of octadecylphosphonic acid ($ODP-H_2$) upon an oxidized silicon substrate, coated with a self-assembled octadecyltrichlorosilane (OTS) monolayer. The molecular area of the $ODP-H_2$ molecules, from pressure *versus* surface area ($\pi - A$) isotherm studies, was determined to be 24.7 ± 2.5 Å^2

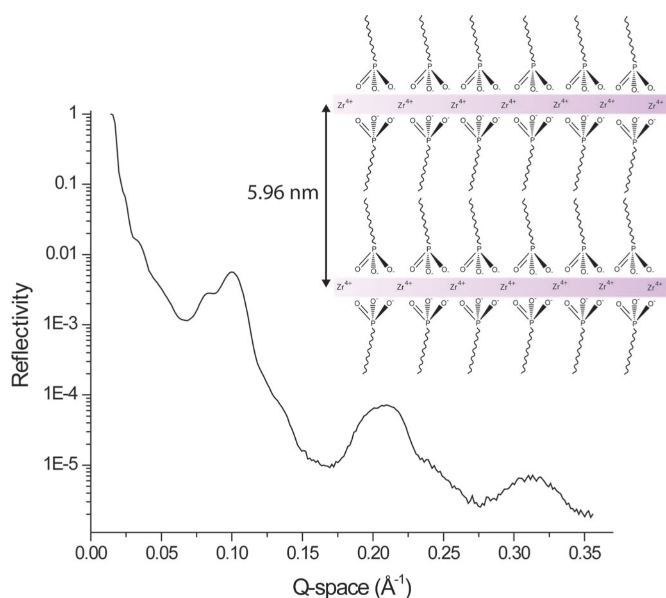

Figure 1. X-ray reflectometry data of multiple zirconium phosphonate bilayers deposited upon an OTS-modified silicon/silicon oxide substrate, showing (001), (002), and (003) reflections at $Q = 0.101$, $Q = 0.207$, and $Q = 0.311$, respectively. Differences in the Q-spacing among the reflections indicates a d spacing of 5.96 nm.

and within the expected range.[21,22] Following the LB deposition of $ODP-H_2$, the phosphonic acid terminated hybrid bilayer was capped with Zr^{4+} ions by exposure to an aqueous solution of $ZrOCl_2 \cdot 8H_2O$ (*ca.* pH 3). The contact angle measurement ($74 \pm 3°$) of the zirconium ion capped octadecylphosphonate (ODP) hybrid bilayer (Si-OTS/ODP-Zr^{4+}) showed a significant decrease in the hydrophobic character of the surface, compared to the starting OTS-modified silicon substrate ($106 \pm 3°$). Ellipsometry measurements were recorded to determine the film thickness and were fitted using a refractive index, n, of 1.460 for the SiO_2-coated silicon substrate and 1.450 for the OTS monolayer.[23] Both the SiO_2 (2.8 nm) and OTS (2.1 nm) thicknesses were independently calculated. Measurements recorded across random regions of the film surface indicated a Zr-ODP layer thickness of 4.5 ± 0.5 nm. This indicates a significant contribution to the observed thickness (*ca.* 2.0 nm) is provided by the Zr^{4+} metal ions bound to the phosphonate headgroups as the expected length of an $ODP-H_2$ molecule is only *ca.* 2.5 nm.[22] The nature of the zirconium-terminated surface resulting from the method employed here is different to that obtained by Talham *et al.*,[21] who observed an ODP film capped with a simple monolayer of Zr^{4+} ions bound to the phosphonate head groups. Additional evidence supporting the presence of a complex polymeric (multilayered) zirconium system at the film surface was provided by XPS analysis. XPS data confirmed the presence of carbon (C 1s, 285.0 eV), oxygen (O 1s, 532.1 eV), phosphorus (P $2p_{3/2}$, 133.8 eV), and zirconium (Zr $3d_{3/2}$, 183.7 eV, $3d_{5/2}$, 185.7 eV), with binding energies referenced to the hydrocarbon C1s peak at 285.0 eV. XPS studies (using takeoff angles of 10°, 30°, and 90°) confirm the film surface to terminate with Zr^{4+} species and an excess of zirconium was identified from the Zr:P ratio (*ca.* 2:1) (see Supporting Information, Table S1). The formation of dif-

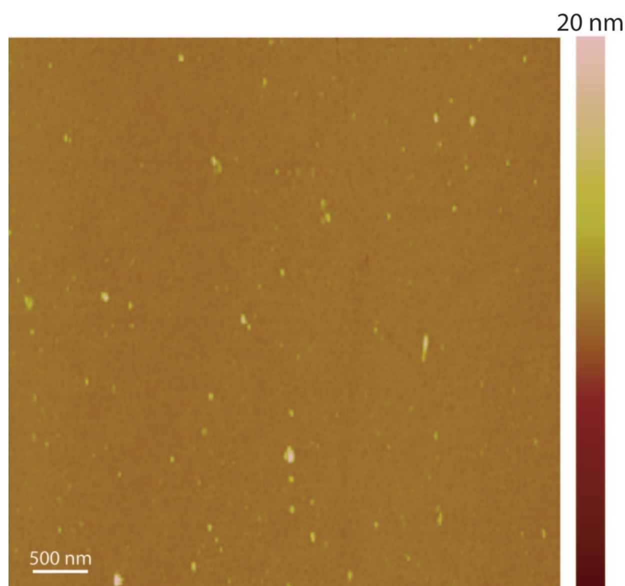

Figure 2. TappingMode AFM height image (5 × 5 μm^2) of zirconium ion stabilizsed hybrid OTS/ODP bilayer on a silicon/silicon oxide substrate.

ferent film types, monolayer with a Zr:P ratio of 1:1 observed by Talham[21] and the polymeric or multilayered film observed in this work, may be rationalized and accounted for by considering the complex nature of aqueous zirconium chemistry which is dominated by the formation of metal−oxygen bonds. The formation of polymeric Zr−O structures readily occurs owing to the highly charged nature of Zr^{4+} ions resulting in their rapid hydrolysis with polymerization typically following. In particular, the hydrolysis of $ZrOCl_2$ to form the hydroxyl-bridged tetrameric cation $[Zr_4(OH)_8(H_2O)_{16}]^{8+}$ and other zirconium hydrous polymers is known.[24–26] However, the occurrence and extent of polymerization is dependent upon several parameters including concentration, pH, temperature, and solution aging.

Further confirmation of the complex nature of the films was obtained from X-ray reflectometry (XRR) analysis of multilayered zirconium octadecylphosphonate films, Figure 1. Multilayer films consisting of seven repeat zirconium octadecylphosphonate bilayers, were prepared through sequential "Y-type" LB deposition of octadecylphosphonic acid monolayers. The periodicity of the film was calculated from the difference in Q-space between the observed Bragg peaks ($d = 2\pi/\Delta Q_z$). The ΔQ value measured among the Bragg peaks corresponds to a d spacing of *ca*. 6.0 nm, arising from the zirconium-capped bilayer structure, repeated throughout the film. This equates to a Zr/ODP thickness of *ca*. 3.5 nm and a Zr^{4+} layer thickness of approximately 1.0 nm, both assuming that the length of an ODP molecule is 2.5 nm. Although these values appear low, when compared to the ellipsometry data for the starting hybrid bilayer, this simple model does not consider the tilt angle of the ODP molecules in the multilayer film or interdigitisation which may occur among the ODP layers. Tilting of the ODP molecules is likely to result in a reduction of the ODP contribution to the 6.0 nm spacing calculated therefore increasing the contribution from the Zr^{4+} layer. A tilt of 30° in the ODP molecule (as observed in some ODP films)[27] would give an effective height of 2.25 nm for a single ODP layer, which if the spacing in the multilayer film is 6.0 nm (as measured) would give a Zr/ODP thickness of 3.75 nm and thus a Zr^{4+} layer thickness of 1.5 nm.

AFM imaging shows the presence of a highly smooth film, with a rms roughness of 0.5 ± 0.1 nm across 5 × 5 μm^2 regions, Figure 2. Further films were prepared, depositing the initial ODP-H_2 monolayer at a surface pressure of 10 mN/m, and with a deposition rate of 10 mm/min. Standard zirconium binding conditions were subsequently followed. These film deposition conditions were employed to deliberately attempt to introduce defects within the film to enable depth profiling by AFM analysis.

AFM imaging of the highly defective films shows the surfaces to consist of "island-like" structures, Figure 3. The significant variations in the depths of the defects

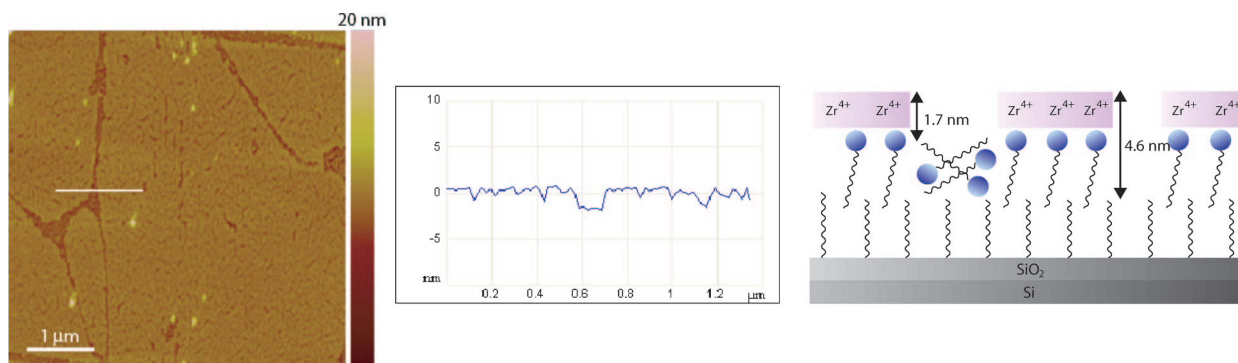

Figure 3. TappingMode AFM height image (5 × 5 μm^2) of a deliberately defected zirconium ion stabilized hybrid OTS/ODP bilayer on silicon/silicon oxide, deposited at 10 mN/m surface pressure (left). The cross section of the film surface indicates regions where zirconium film growth has failed to take place (center). Schematic of deliberately defected film zirconium octadecylphosphonate film is on the right.

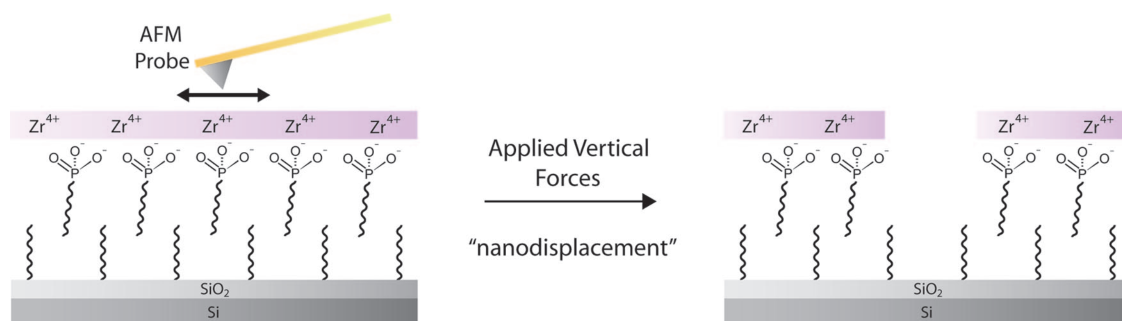

Figure 4. Schematic representation of the selective nanodisplacement by an AFM probe of the upper leaflet of the zirconium-ion-stabilized hybrid OTS/ODP bilayer on silicon/silicon oxide.

(*ca*. 1.7−4.7 nm) are attributed to the high disorder or absence of ODP-H_2 molecules within these regions. Lower defect depths (typically 1.7 ± 0.2 nm) are proposed to arise from ODP-H_2 molecules being present in the defect regions, but orientated in such a manner, that binding of zirconium ions to the phosphonate head groups is prevented or inhibited. Larger defect depths (up to 4.6 ± 0.2 nm) are observed when the ODP-H_2 molecules are highly disordered, lying highly tilted upon the substrate surface, or completely absent. This high disorder/absence of the ODP-H_2 molecules within the defects prevent Zr^{4+} film growth in these regions. The value of 4.6 nm is in close agreement with the Zr-ODP thickness obtained by ellipsometry.

Nanopatterning. In recent years the generation of nanopatterned surfaces has attracted considerable attention.[28,29] The ability to selectively engineer chemical composition and structure on such a small scale is of great potential application, particularly in the fields of nanoelectronics, biotechnology, and sensing. Many lithographic techniques have been developed over the years with photolithography[30−32] and electron beam lithography perhaps the most common.[33] However, other more cost-effective lithographic methods such as microcontact printing,[34,35] mechanical spotting,[36] and nanoimprint lithography[37] continue to develop and find commercial use. Such delivery methods have proved useful in the development and fabrication of DNA,[38] protein,[39] and glyco[40] arrays. More recently, nanolithography methods, based on scanning probe technology (AFM, STM, and SNOM) have been developed,[41] taking advantage of the nanometer-sized dimensions of the probes and strong localized tip−surface interactions. Examples include dip-pen nanolithography,[42] catalytically active AFM probes to induce surface reactions,[43,44] and STM based lithography where high tunnelling currents are used to modify terminal groups or displace surface-bound molecules.[45,46] Similarly, a UV laser coupled to a SNOM can be used to modify surface groups to generate nanoscale patterns.[47] Other examples include nanoshaving and nanografting which rely largely on the physical displacement of molecules by an AFM probe.[48] "Nanoshaving" of monolayers through the application of high vertical forces to the monolayer surface with an AFM probe has previously been demonstrated upon monolayers prepared on both Au[49] and SiH[50] substrates.

Here, using a method similar to that of Liu,[49] we demonstrate for the first time the selective "nanodisplacement" or etching of a substrate supported bilayer system, in which careful control of the vertical forces generated by the AFM probe allows for selective removal of the upper bilayer leaflet, exposing the underlying layer within spacially defined etched regions, Figure 4.

For the inorganic−organic bilayer system Si-OTS/ODP-Zr^{4+} a minimum vertical force threshold of *ca*. 40 nN was required for etching of the upper bilayer surface to generate the nanoscale patterns.[51] Figure 5 shows a typical pattern, in this case a cross, which can be etched into the bilayer film. The bars of the cross are 310 nm in width and 3 μm in length for the bar running from top left to bottom right and 120 nm in width and 3 μm in length for the bar running from top right to bottom left. AFM analysis of such etched regions shows features typically 4.6 ± 0.4 nm in depth. The depth of these features are consistent with the removal of the ODP layer (*ca*. 2.5 nm) and a polymeric Zr^{4+} film of *ca*. 2.1 nm with exposure of the underlying hydrocarbon chains of OTS. Scan rates of 10−12 Hz were typically employed during the nanodisplacement process with complete etching of the desired region achieved rapidly.

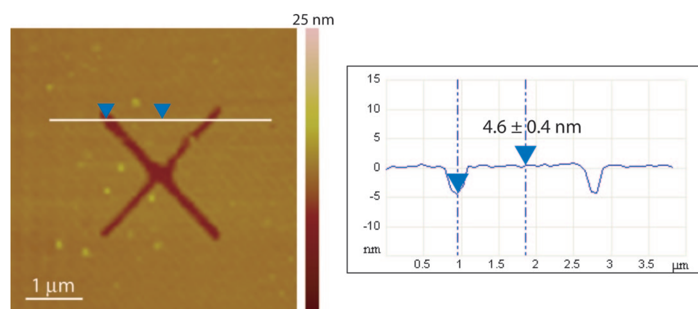

Figure 5. Contact mode AFM height image and cross section of a nanoscale patterned region on the zirconium-ion-stabilized OTS/ODP bilayer deposited on silicon/silicon oxide.

Increasing the etching time to longer periods was found to have no effect upon the depth of the

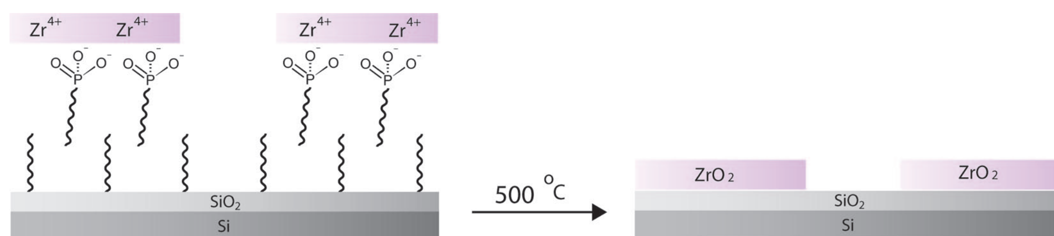

Figure 6. Schematic representation of the formation of the nanopatterned ZrO_2 film following the annealing of the zirconium ion stabilized OTS/ODP bilayer at 500 °C.

etched features. Likewise, increasing the forces applied to the bilayer to values greater than 120 nN were found to have no further effect upon the depth of the etched features. The consistent hole depths observed when varying the applied forces, at values above the etching threshold, suggests that the underlying OTS monolayer remains intact. The inability to etch a silicon-supported OTS monolayer has been observed by Wang et al.[23] who demonstrated that applied forces of up to 1 μN were unable to disrupt the OTS film. Our own attempts to etch silicon-supported OTS monolayers (without an ODP monolayer deposited on top), using force up to *ca.* 240 nN showed similar findings. The high stability of the OTS monolayer, preventing it from being etched, is thought to arise simply from the strong covalent interaction of the OTS molecules with the SiO_2 surface and the high degree of cross-linking which occurs between the monolayer molecules. Repeated scanning of the bilayer surface in contact mode with forces optimized for imaging showed no immediate damage to the film.

The morphology of the etched features proved to be highly stable with complete structural retention of patterned areas observed following exposure to a variety of aqueous and nonaqueous (e.g., dichloromethane, chloroform, ethanol, and hexane) solvents. Structural retention was also observed following heating of patterned bilayers in solvents, to temperatures of 80 °C. Further work is currently underway to investigate the binding of biomolecules and nanoparticles in the hydrophobic pocket generated.

Zirconium Oxide Thin-Film Formation. As the binding of Zr^{4+} ions upon a silicon-supported OTS/ODP hybrid bilayer leads to the formation of a uniform polymeric film, in which zirconium ions are bridged *via* hydroxyl linkages, it can potentially be used to generate metal oxide films of a nanometer-scale thickness, Figure 6. High temperature annealing (500 °C) of the bilayer was found to successfully remove the organic components of the film leaving behind a zirconium oxide (ZrO_2) layer on the substrate surface. Varying the annealing time between 2 and 16 h was found to have no effect upon the quality of the film produced. AFM analysis of the ZrO_2 film reveals a largely uniform surface with an rms roughness of 0.3 ± 0.1 nm over 5 × 5 μm^2 regions, Figure 7. AFM analysis of patterned bilayer surfaces showed a high level of retention of the etch features following annealing, Figure 8. Cross sectional analysis of such etched regions indicated the presence of a 1.6 nm oxide film with an rms roughness similar to before (0.3 ± 0.1 nm). Contact angle analysis indicated the presence of a highly hydrophilic surface, as expected, with consistent values of 32 ± 3°. The formation of the ZrO_2 film is likely to occur *via* the hydrolysis of the zirconyl chloride to zirconium hydrous polymers which are bound to the phosphonate bilayer on the substrate surface. These polymers which are believed to have rodlike morphology,[26] with a high degree of branching depending on pH, then aggregate on heating or aging transforming into a film of ZrO_2 at elevated temperatures. Although direct analysis of the metal oxide film by grazing angle X-ray diffraction was not successful, variable temperature X-ray diffraction of the zirconium precursor $ZrOCl_2$, exposed to water and dried, showed the onset of crystallization of tetragonal (high temperature form) ZrO_2 at *ca.* 290 °C with peaks sharpening on warming to 900 °C. Upon cooling back to room temperature both the monoclinic and tetragonal forms of ZrO_2 are present (see

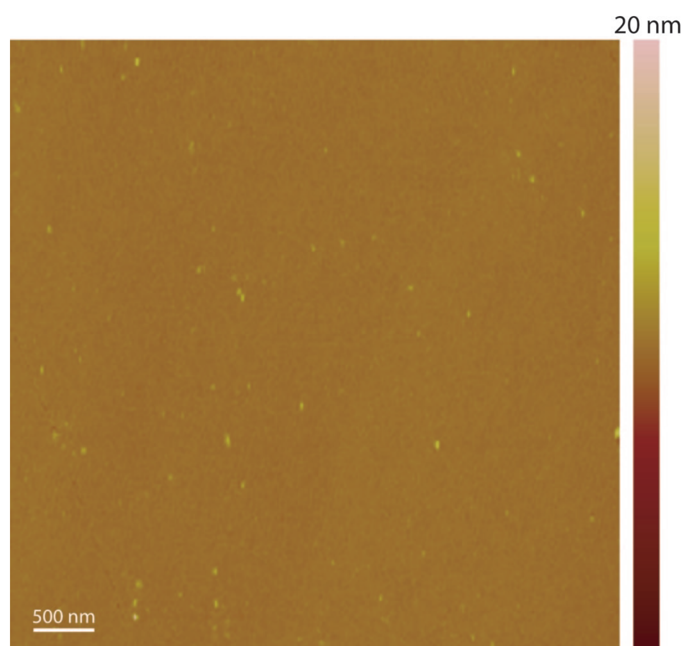

Figure 7. Contact mode AFM height image (5 × 5 μm^2) of a ZrO_2 film on a silicon/silicon oxide substrate surface following the annealing of the zirconium-ion-stabilized OTS/ODP bilayer at 500 °C.

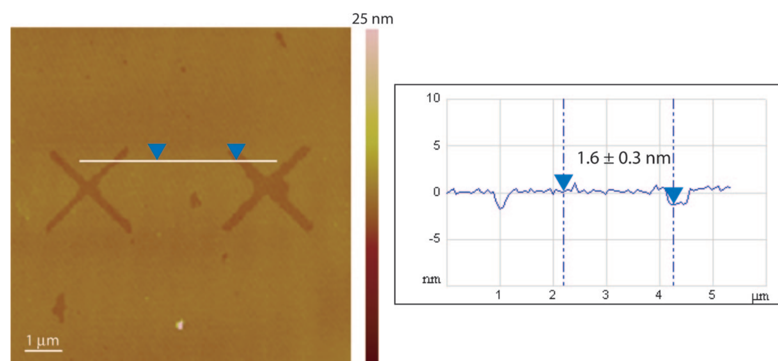

Figure 8. Contact mode AFM height image and cross section of a nanoscale patterned ZrO_2 film, on silicon/silicon oxide, formed following the annealing of the zirconium-ion-stabilized OTS/ODP bilayer at 500 °C.

Supporting Information Figure S1 and Figure S2), confirming the likely formation of ZrO_2 following the annealing of the bilayer Si-OTS/ODP-Zr^{4+} at 500 °C.

CONCLUSIONS

Zirconium-ion-stabilized bilayers of ODP/OTS, prepared by metal-binding and Langmuir–Blodgett methods, have been shown to contain a polymeric film of hydroxyl bridged Zr^{4+} ions on the surface of approximately 2 nm thick. Nanoscale patterns can be introduced into the bilayer using nanodisplacement methodology where the upper layer of ODP can be removed by careful control of the forces exerted by an AFM probe to generate hydrophobic OTS terminated regions on an otherwise hydrophilic surface. In addition, the metal stabilized bilayer can be subsequently annealed to generate patterned or unpatterned nanometer thick (*ca*. 1.6 nm), highly uniform zirconium oxide films.

EXPERIMENTAL METHODS

Materials. Reagents were obtained from commercial sources and used as supplied. Octadecyltrichlorosilane (OTS, $C_{18}H_{37}SiCl_3$, 95%) and zirconyl (IV) chloride octahydrate ($ZrOCl_2 \cdot 8H_2O$, 98%) were purchased from Acros Organics. Octadecylphosphonic acid (ODP-H_2, $C_{18}H_{37}PO_3H_2$, 93+ %) was purchased from Alfa Aesar. High purity water with a resistivity of 18 MΩcm (Neptune purification system, Purite) was used for all experiments. Si (111) wafers (100 mm diameter, 1.0182–2.2675 Ωcm resistivity; 500–550 µm thick) were purchased from Cemat Silicon S. A. (Warsaw, Poland). Prior to use, the silicon wafers were sonicated for 20 min in acetone, followed by rinsing with high purity water. They were then treated in piranha solution (3:1 H_2O_2/H_2SO_4) for 45 min at 80 °C and rinsed thoroughly with high purity water [Warning: piranha solution should be handled with extreme care; it is a strong oxidant and reacts violently with many organic materials. It also presents an explosion danger]. Finally, the silicon wafers were immersed in a 1:1 H_2O_2/HCl solution for 15 min at room temperature then rinsed with copious amounts of high purity water and dried in air at 110 °C.

Monolayer Formation. Monolayer modification was carried out on cleaned silicon wafers by immersion in a 1 mM octadecyltrichlorosilane (OTS) solution, prepared in dry toluene, for 48 h. Following monolayer formation, wafers were sonicated in 2 × 15 mL of toluene, followed by 2 × 15 mL of $CHCl_3$ for 10 min each, and given a final rinse with copious amounts high purity water.

Bilayer Formation. Langmuir–Blodgett (LB) deposition of octadecylphosphonic acid (ODP-H_2) films upon OTS-modified silicon substrates was performed on a 611D Teflon-coated Langmuir dipping trough (Nima Instruments, Coventry, U.K.) equipped with a PTFE barrier and a DL1 dipping mechanism and a Wilhelmy plate PS4 pressure sensor equipped with filter paper strips (1 × 2 cm^2) to measure the surface pressure. Single-barrier "pressure *versus* area" (π–A) Langmuir isotherms were recorded using Nima Instruments Langmuir Trough software, version 5.16. High purity water (18 MΩcm) was used for the subphase in the Langmuir trough. A glass sample vial was placed under the subphase in the well of the trough. Octadecylphosphonic acid was spread on the subphase typically from 0.3–0.5 mg/ml $CHCl_3$ solutions and left for 15 min to allow solvent evaporation. The film was compressed at a rate of 40 cm^2/min to a target surface pressure of 20 mN/m *via* 1.5 isotherm compression cycles. Film transfer was achieved by passing the hydrophobic substrate through the subphase-supported monolayer into the sample vial at a rate of 8 mm/min, while maintaining the target surface pressure. The remaining monolayer film upon the subphase was removed by vacuum suction, and the barrier opened. The substrate and vial were removed from the trough and zirconyl chloride was added to the vial to a concentration of *ca*. 0.5 mM. The substrates remained immersed in the Zr^{4+} solution for 1 h. Following Zr^{4+} treatment, the now hydrophilic substrate was removed from the sample vial and washed thoroughly with 2 × 15 mL of high purity water.

Multilayer Formation. Following the formation of the hybrid bilayer subsequent layers of ODP-H_2 were deposited by withdrawing the substrate from the subphase, at a rate of 8 mm/min, while maintaining the target surface pressure of 20 mN/m followed by passing the now hydrophobic substrate back through the subphase-supported monolayer into a sample vial. The substrate and vial were then removed from the trough, and zirconyl chloride was added to a concentration of *ca*. 0.5 mM. The substrate remained immersed in the Zr^{4+} solution for 1 h after which time it was removed and washed thoroughly with 2 × 15 mL of high purity water. The process was then repeated for additional layers.

Atomic Force Microscopy. AFM imaging of monolayers and hybrid bilayers was carried out in both contact and TappingMode on a Multimode AFM equipped with a NanoscopeIV controller (Veeco Instruments Inc., California USA). Contact mode operation was carried out using sharpened silicon nitride tips (NPS) with a cantilever spring constant of 0.58 N/m (Veeco Instruments Ltd., Cambridge, UK). TappingMode operation was carried out with etched silicon probes (OTESPA), with a spring constant of 42 N/m (Veeco Instruments Ltd., Cambridge, U.K.). Nanopatterning/nanodisplacement was carried out in contact mode using sharpened silicon nitride tips with a cantilever spring constant of 0.58 N/m and a tip radius of 20–60 nm.

XPS Measurements. X-ray photoelectron spectroscopy (XPS) was carried out using a Scienta ESCA 300 with an Al Kα X-ray source (1486.6 eV) at the National Centre for Electron Spectroscopy and Surface Analysis (NCESS), Daresbury Laboratory, U.K. Take off angles of 10°, 30°, and 90° were used for analysis of each sample. The modified silicon substrates were mounted on sample stubs with conductive carbon tape. All peaks were fitted with Gaussian–Lorentz peaks using in-house software to obtain peak area information. A linear baseline was used in fitting processes.

Ellipsometry Measurements. Film thickness measurements were carried out using a SE 500 Model ellipsometer (Sentech Instruments GmbH, Berlin, Germany) employing an angle of incidence of 70° with a He Ne laser, $\lambda = 632.8$ nm, as the light source. Film thickness values were calculated from n, Ψ, and Δ using simulation software accompanying the SE 500. The refractive index, n, of the OTS monolayers was assumed to be the same as that of the monolayer precursor molecule ($n = 1.450$). The sili-

con oxide layer on the silicon wafers was measured on the SE 500, prior to measurement of monolayer thickness, using an assumed refractive index of $n = 1.460$.

X-Ray Reflectometry. Thickness measurements of monolayers and multilayers on silicon wafers were carried out by X-ray reflectometry with a D5000 Diffractometer (Siemens, Germany) using a graphite monochromated Cu Kα, $\lambda = 1.5418$ Å, X-ray source. Data collection and processing was performed using software accompanying the D5000.

Contact Angle Measurements. Static contact angle measurements were carried out using the sessile drop method at room temperature with a Rame-Hart (Mountain Lakes, NJ) NRL model 100-00 contact angle goniometer. A micropipet was used to dispense 2 µl of probe droplets of high purity water to the sample surface.

Acknowledgment. We thank Dr. G. Beamson of the National Centre for Electron Spectroscopy and Surface Analysis (NCESS) at Daresbury Laboratory for technical assistance and useful discussions on the XPS measurements, Prof. J. Evans for recording the XRD data, Dr. R. Thompson for help with XRR, and the EPSRC (studentship for S.M.D.W. and grant EP/E025722/1 for XPS facilities) for funding.

Supporting Information Available: The variable temperature X-ray diffraction pattern of hydrolyzed $ZrOCl_2$; Figure S1 and Figure S2; data for the Zr/P ratio obtained from XPS, Table S1. This material is available free of charge *via* the Internet at http://pubs.acs.org.

REFERENCES AND NOTES

1. Cameron, M. A.; George, S. M. ZrO_2 Film Growth by Chemical Vapor Deposition Using Zirconium Tetra-*tert*-Butoxide. *Thin Solid Films* **1999**, *348*, 90–98.
2. Kingon, A. I; Maria, J-P.; Streiffer, S. K. Alternative Dielectrics to Silicon Dioxide for Memory and Logic Devices. *Nature* **2000**, *406*, 1032–1038.
3. Copel, M.; Gribelyuk, M.; Gusev, E. Structure and Stability of Ultrathin Zirconium Oxide Layers on Si(001). *Appl. Phys. Lett.* **2000**, *76*, 436–438.
4. Chang, J. P.; Lin, Y. S. J. Highly Conformal ZrO 2 Deposition for Dynamic Random Access Memory Application. *Appl. Phys.* **2001**, *90*, 2964–2969.
5. Cassir, M.; Goubin, F.; Bernay, C.; Vernoux, P.; Lincot, D. Synthesis of ZrO_2 Thin Films by Atomic Layer Deposition: Growth Kinetics, Structural and Electrical Properties. *Appl. Surf. Sci.* **2002**, *193*, 120–128.
6. Ehrhart, G.; Capoen, B.; Robbe, O.; Boy, P.; Turrell, S,; Bouazaoui, M. Structural and Optical Properties of *n*-Propoxide Sol-Gel Derived ZrO_2 Thin Films. *Thin Solid Films* **2001**, *496*, 227–233.
7. Khawaja, E. E.; Bouamrane, F.; Hallak, A. B.; Daous, M. A.; Salim, A. M. Observation of Oxygen Enrichment in Zirconium Oxide Films. *J. Vac. Sci. Technol., A* **1993**, *11*, 580–587.
8. Zhao, Z. W.; Tay, B. K.; Huang, L.; Yu, G. Q. Study of the Structure and Optical Properties of Nanocrystalline Zirconium Oxide Thin Films Deposited at Low Temperatures. *J. Phys. D: Appl. Phys.* **2004**, *37*, 1701–1705.
9. Ben Amor, S.; Rogier, B.; Baud, G.; Jacquet, M.; Nardin, M. Characterization of Zirconia Films Deposited by R.F. Magnetron Sputtering. *Mater. Sci. Eng., B* **1998**, *57*, 28–39.
10. Brugger, A.; Schoppmann, C.; Schurr, M.; Seidl, M.; Sipos, G.; Hahn, C. Y.; Hassmann, J.; Waldmann, O.; Voit, H. Ultrathin Fe-Oxide Layers Made from Langmuir-Blodgett Films. *Thin Solid Films* **1998**, *338*, 231–242.
11. Mirley, C. L.; Koberstein, J. T. Preparation of Ultrathin Metal Oxide Films from Langmuir−Blodgett Layers. *Langmuir* **1995**, *11*, 2837–2839.
12. Matsuura, N.; Johnson, D. J.; Amm, D. T. Fabrication of Cadmium Oxide Thin Films Using the Langmuir−Blodgett Deposition Technique. *Thin Solid Films* **1997**, *295*, 260–265.
13. Taylor, D. M.; Lambi, J. N. On the Preparation of Thin Metal Oxides by Langmuir−Blodgett Film Deposition. *Thin Solid Films* **1994**, *243*, 384–388.
14. Paranjape, D. V.; Sastry, M.; Ganguly, P. Deposition of Thin Films of TiO_2 from Langmuir−Blodgett Film Precursors. *Appl. Phys. Lett.* **1993**, *63*, 18–20.
15. Amm, D. T.; Johnson, D. J.; Laursen, T.; Gupta, S. K. Fabrication of Ultrathin Metal Oxide Films Using Langmuir−Blodgett Deposition. *Appl. Phys. Lett.* **1992**, *61*, 522–524.
16. Gang, Z.; Kun, F.; Pingsheng, H.; Haizeng, S. Preparation of Y_2O_3 -Stabilized ZrO_2 Thin Electrolyte Films from Langmuir−Blodgett Film Precursors by Means of "Surface Ions". *J. Mater. Chem.* **2002**, *12*, 2998–3002.
17. Seip, C. T.; Talham, D. R. Organic/Inorganic Langmuir−Blodgett Films Based on Known Layered Solids: Characterization and Reaction of Cobalt Octadecylphosphonate. *Mater. Res. Bull.* **1999**, *34*, 437–445, and references therein.
18. Lee, H.; Kepley, L. J.; Hong, H.-G.; Mallouk, T. E. Inorganic Analogs of Langmuir-Blodgett Films: Adsorption of Ordered Zirconium 1,10-Decanebisphosphonate Multilayers on Silicon Surfaces. *J. Am. Chem. Soc.* **1988**, *110*, 618–620.
19. Lee, H.; Kepley, L. J.; Hong, H.-G.; Akhter, S.; Mallouk, T. E. Adsorption of Ordered Zirconium Phosphonate Multilayer Films on Silicon and Gold Surfaces. *J. Phys. Chem.* **1988**, *92*, 2597–2601.
20. Putvinski, T. M.; Schilling, M. L.; Katz, H. E.; Chidsey, C. E. D.; Mujsce, A. M.; Emerson, A. B. Self-Assembly of Organic Multilayers with Polar Order Using Zirconium Phosphate Bonding between Layers. *Langmuir* **1990**, *6*, 1567–1571.
21. Byrd, H.; Pike, J.K.D. R; Talham, D. R. Inorganic Monolayers Formed at an Organic Template: a Langmuir-Blodgett Route to Monolayer and Multilayer Films of Zirconium Octadecylphosphonate. *Chem. Mater.* **1993**, *5*, 709–715.
22. Woodward, J. T.; Ulman, A.; Schwartz, D. K. Self-Assembled Monolayer Growth of Octadecylphosphonic Acid on Mica. *Langmuir* **1996**, *12*, 3626–3629.
23. Wang, M.; Liechti, K. M.; Wang, Q.; White, J. M. Self-Assembled Silane Monolayers: Fabrication with Nanoscale Uniformity. *Langmuir* **2005**, *21*, 1848–1857.
24. Devia, D. H.; Sykes, A. G. Aqueous Solution Chemistry of Zirconium(IV). 1. Kinetic Studies on Hydrogen Ion and General Acid (HX) Induced Dissociations of the Tetrameric ion $[Zr_4(OH)_8(H_2O)_{16}]^{8+}$. *Inorg. Chem.* **1981**, *20*, 910–913.
25. Clearfield, A. Structural Aspects of Zirconium Chemistry. *Rev. Pure Appl. Chem.* **1964**, *14*, 91–108.
26. Singhal, A.; Toth, L. M.; Beaucage, G.; Lin, J-S.; Peterson, J. Growth and Structure of Zirconium Hydrous Polymers in Aqueous Solutions. *J. Colloid Interface Sci.* **1997**, *194*, 470–481.
27. Byrd, H.; Whipps, S.; Pike, J. K.; Ma, J.; Nagler, S. E.; Talham, D. R. Role of the Template Layer in Organizing Self-Assembled Films: Zirconium Phosphonate Monolayers and Multilayers at a Langmuir−Blodgett Template. *J. Am. Chem. Soc.* **1994**, *116*, 295–301.
28. Wollman, E. W.; Kang, D.; Frisbie, C. D.; Lorkovic, I. M.; Wrighton, M. S. Photosensitive Self-Assembled Monolayers on Gold: Photochemistry of Surface-Confined Aryl Azide and Cyclopentadienylmanganese Tricarbonyl. *J. Am. Chem. Soc.* **1994**, *116*, 4395–4404.
29. Kumar, A.; Abbott, N. L.; Kim, E.; Biebuyck, H. A.; Whitesides, G. M. Patterned Self-Assembled Monolayers and Meso-Scale Phenomena. *Acc. Chem. Res.* **1995**, *28*, 219–226.
30. Xia, Y. N.; Whitesides, G. M. Soft Lithography. *Angew. Chem., Int. Ed.* **1998**, *37*, 551–575.
31. Gates, B. D.; Xu, Q.; Love, J. C.; Wolfe, D. B.; Whitesides, G. M. Unconventional Nanofabrication. *Annu. Rev. Mater. Res.* **2004**, *34*, 339–372.
32. Solak, H. H. Nanolithography with Coherent Extreme Ultraviolet Light. *J. Phys. D: Appl. Phys* **2006**, *39*, R171R188 and references therein.
33. Chen, W.; Ahmed, H. Fabrication of 5−7 nm Wide Etched Lines in Silicon Using 100 keV Electron-Beam Lithography and Polymethylmethacrylate Resist. *Appl. Phys. Lett.* **1993**, *62*, 1499–1501.

34. Kumar, A.; Whitesides, G. M. Patterned Condensation Figures as Optical Diffraction Gratings. *Science* **1994**, *263*, 60–62.
35. Delamarche, E.; Geissler, M.; Wolf, H.; Michel, B. Positive Microcontact Printing. *J. Am. Chem. Soc.* **2002**, *124*, 3834–3835.
36. Schena, M.; Theriault, T. P.; Konrad, K.; Lachenmeier, E.; Davis, R. W. Microarrays: Biotechnology's Discovery Platform for Functional Genomics. *Trends Biotechnol.* **1998**, *16*, 301–306.
37. Guo, L. J. Recent Progress in Nanoimprint Technology and its Applications. *J. Phys. D: Appl. Phys.* **2004**, *37*, R123–R141.
38. Pirrung, M. C.; Bradley, J. Dimethoxybenzoin Carbonates: Photochemically-Removable Alcohol Protecting Groups Suitable for Phosphoramidite-Based DNA Synthesis. *J. Org. Chem.* **1995**, *60*, 1116–1117.
39. Schweitzer, B.; Predki, P.; Snyder, M. Microarrays to Characterize Protein Interactions on a Whole-Proteome Scale. *Proteonomics* **2003**, *3*, 2190–2199.
40. Fazio, F.; Bryan, M. C.; Blixt, O.; Paulson, J. C.; Wong, C.-H. Synthesis of Sugar Arrays in Microtiter Plate. *J. Am. Chem. Soc.* **2002**, *124*, 14397–14402.
41. Kramer, S.; Fuierer, R. R.; Gorman, C. B. Scanning Probe Lithography Using Self-Assembled Monolayers. *Chem. Rev.* **2003**, *103*, 4367–4418.
42. Piner, R. D.; Zhu, J.; Xu, F.; Hong, S. H.; Mirkin, C. A. "Dip-Pen" Nanolithography. *Science* **1999**, *283*, 661–663.
43. Davis, J. J.; Coleman, K. S.; Busuttil, K. L.; Bagshaw, C. B. Spatially Resolved Suzuki Coupling Reaction Initiated and Controlled Using a Catalytic AFM Probe. *J. Am. Chem. Soc.* **2005**, *127*, 13082–13083.
44. Davis, J. J.; Bagshaw, C. B.; Busuttil, K. L.; Hanyu, Y.; Coleman, K. S. Spatially Controlled Suzuki and Heck Catalytic Molecular Coupling. *J. Am. Chem. Soc.* **2006**, *128*, 14135–14141.
45. Marrian, C. R. K.; Perkins, F. K.; Brandow, S. L.; Koloski, T. S.; Dobisz, E. A.; Calvert, J. M. Low Voltage Electron Beam Lithography in Self-Assembled Ultrathin Films with the Scanning Tunneling Microscope. *App. Phys. Lett.* **1994**, *64*, 390–392.
46. Mizutani, W.; Ishida, T.; Tokumoto, H. Nanoscale Reversible Molecular Extraction from a Self-Assembled Monolayer on Gold(111) by a Scanning Tunneling Microscope. *Langmuir* **1998**, *14*, 7197–7202.
47. Sun, S.; Chong, K. S. L.; Leggett, G. J. Nanoscale Molecular Patterns Fabricated by Using Scanning Near-Field Optical Lithography. *J. Am. Chem. Soc.* **2002**, *124*, 2414–2415.
48. Liu, G. Y.; Xu, S.; Qian, Y. L. Nanofabrication of Self-Assembled Monolayers Using Scanning Probe Lithography. *Acc. Chem. Res.* **2000**, *33*, 457–466.
49. Xu, S.; Liu, G. Nanometer-Scale Fabrication by Simultaneous Nanoshaving and Molecular Self-Assembly. *Langmuir* **1997**, *13*, 127–129.
50. Headrick, J. E.; Armstrong, M.; Cratty, J.; Hammond, S.; Sheriff, B. A.; Berrie, C. L. Nanoscale Patterning of Alkyl Monolayers on Silicon Using the Atomic Force Microscope. *Langmuir* **2005**, *21*, 4117–4122.
51. If the tip radius is assumed to be 20 nm, a displacement force of 40 nN corresponds to a pressure of 31.8 MPa.